ACS OMEGA

Open Access

http://pubs.acs.org/journal/acsodf

Article

Development of Fluorescent Co (II)-Integrated Carbon Dots and Their Application as a Off−On Mesotrione Detection Sensor

Rani, Faiz Ali,* Mian Muhammad, and Zeid A. AlOthman

Cite This: *ACS Omega* 2023, 8, 49115−49128

Read Online

ACCESS | Metrics & More | Article Recommendations | Supporting Information

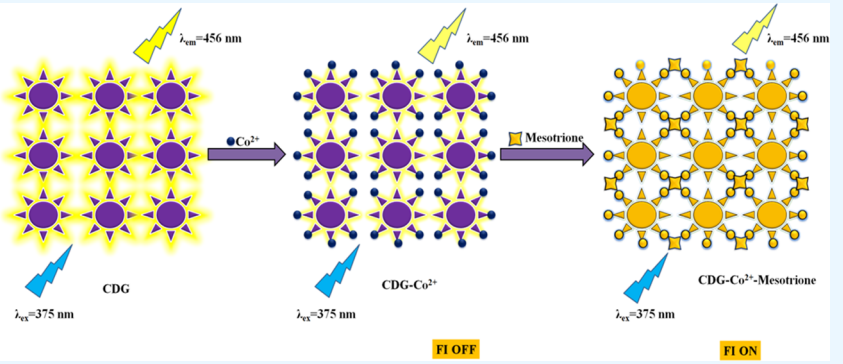

ABSTRACT: A very simple mesotrione-sensing medium with enhanced sensitivity detection limits has been proposed. A renovated hydrothermal method was adopted for synthesizing fluorescent carbon dots from ethylenediamine and glucose using a Teflon-lined simple autoclave in a GC oven. The resultant carbon dots were characterized via TEM, FTIR, UV−vis, particle size distribution, and EDX and evaluated in a fluorimeter as the sensing medium for mesotrione detection. The binding approach of the Co (II)-integrated glucose-bound carbon dots toward mesotrione is selective, making them an effective sensor for the real sample applications, where majority of the coexisting substances showed insignificant interference effect. Formation of the metastable state due to the molecular interaction between carbon dots and Co (II) resulted in fluorescence quenching at 456 nm. Enhancement in the fluorescence intensity occurred when mesotrione was added in the concentration range of 0.2−5.0 μg mL^{-1}, with a limit of detection, limit of quantification, standard deviation, and relative standard deviation of 0.054, 0.164, 0.00082 μg mL^{-1}, and 0.682%, respectively. Mesotrione determination was demonstrated in soil, water, and tomato samples with recoveries in the range of 95.38−104.7%. The selectivity of the sensor was found to be good enough when checked for the complex tomato sample spiked with different pesticides of the triketone family having structural similarities to mesotrione.

1. INTRODUCTION

In modern agriculture, pesticides find a crucial place in mitigating the adverse effects of pests and weeds, ensuring a steady and sufficient food supply to the ever-expanding global population.[1] However, it is imperative to acknowledge that even at low concentrations the residual presence of pesticides can pose significant threats to the environment and overall health of living organisms worldwide.[1,2] Consequently, there is a pressing need for precise, reliable, and swiftly validated analytical protocols and strategies to accurately determine pesticide concentrations.[3−13]

Mesotrione (2-(4-(methylsulfonyl)-2-nitrobenzoyl)-1,3-cyclohexanedione) belongs to the triketone herbicide family and serves as an effective pre- and post emergence herbicide, specifically safeguarding maize crops against broadleaf, annual grass weeds, and certain gramineous weeds. Undoubtedly, mesotrione plays a crucial role in agricultural production, but the persistence of its residues in the soil/water can lead to detrimental consequences for sensitive crops and pose drastic hazards to human and animal health. Consequently, the detection of mesotrione residues by developing sensitive, easy, selective, and cost-effective analytical methods and strategies acquires significance.[14−19]

To date, numerous detection methods have been reported for the detection of mesotrione, including liquid chromatography mass spectrometry,[17] solid-phase microextraction,[20] enzyme-linked immunosorbent assay,[21] mass spectrometry,[22,23] high-performance liquid chromatography (HPLC),[23] square wave voltammetry, fluorimmuno assay, spectrophotometric method, diode array detection and cyclic voltammetry,

Received: September 19, 2023
Revised: November 27, 2023
Accepted: December 5, 2023
Published: December 13, 2023

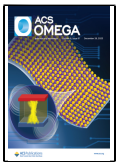

and differential pulse voltammetry. A short comparison of those methods is given in Table S1. Among these techniques, HPLC remains the most employed method for mesotrione detection and analysis.[23] The limitations associated with these methods such as prolonged analysis time, difficulty in sample preparation, complicated usage, need of costly and sophisticated instruments, and the availability of skilled technicians[24] compelled the researchers to search for methods/strategies with least shortcomings. Developing a new method for the sensitive, rapid, selective, and simple quantification of mesotrione poses a significant challenge.[24] It is essential to solve these constraints to develop a mesotrione detection approach that is more reliable and practical. However, optical analysis methods present a promising alternative for pesticide analysis due to their simple instrumentation, shorter response time, cost effectiveness, and ease of operation.

Fluorescence-based sensors utilizing various materials such as quantum dots, metal organic frameworks, fluorescent proteins, and organic dyes have been reported for the determination of pesticides.[25,26] Comparison of the sensors and sensing media is summarized in Table S2.

In 2004, during the cleaning process of single-walled carbon nanotubes (SWCNTs), carbon dots (CDs) were discovered accidentally.[27] These CDs bear structural similarities to quantum dots and belong to the class of zero-dimensional carbon nanoparticles, exhibiting an amorphous to nanocrystalline structure with a small particle diameter less than 10 nm. CDs possess a sp^3-bonded carbon skeleton like that of graphite oxide particles.[27−29] They are made up of a crystalline graphitic core, which is surrounded by several functional groups that contribute to their water solubility.

Since their fortuitous discovery in the early 2000s, carbon dots have been considered as a green alternative to the traditional quantum dots.[30] These nanomaterials consist of oxygen and nitrogen-based groups as well as modified functional groups, facilitating easy interaction/binding with analyte molecules.[27−31] Fluorescent nanoparticles from the family of carbon nanomaterials are ideal bioimaging probes because of their strong biocompatibility and potentially lower cytotoxicity when compared to semiconductor quantum dots.

The remarkable properties of CDs, such as low toxicity, stability, high biocompatibility, broad excitation/emission range, photoluminescence (PL), easy functionalization, utilization of low-cost precursors, enhanced solubility, facile synthesis, and brightness, have made them widely applicable in various fields.[1,2,32−42] Notably, the fluorescence emission characteristic of carbon dots (CDs) renders them particularly appealing as sensing media in fluorescence-based sensing.

Carbon-dot-based sensors have shown promising capabilities in detecting various metal ions, including Cu^{2+}, K^+, Hg^{2+}, and Ag^+. Additionally, they have been reported for the detection of materials and different biological agents, such as viruses, bacteria, and various pathogenic organisms. However, the application of carbon-dot-based systems as sensing media for pesticide detection could not get the desired attention and this field of research is still in its evolutionary phase.[43,44]

Glucose-containing carbon dots (CDG) were synthesized from glucose and ethylenediamine via the renovated hydrothermal protocol and incorporation of a simple Teflon-lined autoclave using a GC oven instead of a conventional autoclave. Only two articles report on the specific fluorescence detection of mesotrione,[14,45,46] but the current study demonstrates a very simple, direct, and cost-effective fluorescence method for the highly specific detection of mesotrione, which much improved analytical and statistical parameters such as regression coefficient, % recovery, LOQ, and % RSD. The CDGs came out with good results when checked for MST determination. The synthesized CDGs exhibited excellent porous and fluorescent properties, leading to stable fluorescent intensity (FI) in aqueous media. In the presence of Co(II), the FI of CDGs was quenched owing to the formation of a metastable fluorescent ground-state complex, CDG-Co(II). Notably, the addition of MST to the solution containing CDG-Co(II) led to the enhancement of FI, confirming the results of this procedure with improved sensing capabilities. To thoroughly assess performance of the newly proposed system, various physical and chemical parameters including concentration of CDG and Co (II), pH, time, and the potential interferences of other pesticides and metal ions were investigated. Under optimized conditions, the proposed method was rigorously validated using statistical parameters and analytical figures of merit to ensure its reliability. The analytically validated approach was successfully applied to determine MST concentrations in spiked and different real environmental samples.

2. EXPERIMENTAL SECTION

2.1. Chemicals and Materials. Mesotrione, pirimicarb (PRC), atrazine (At), chlortoluron (Chl), imidacloprid (Imd), methomyl (MT), and carbofuran (CB), sulcotrione, tembotrione, and benzofenap were purchased from (Sigma-Aldrich, Germany) as their technical standards. While boric acid (ACS reagent grade), phosphoric acid (85%), NaOH, cobalt(II) chloride, cadmium(II) chloride, chromium nitrate, copper acetate, silver nitrate, magnesium sulfate, sodium chloride, calcium chloride, and monolith grade acetic acid (ACS reagent) were purchased from Phillipsburg, NJ.

2.2. Instrumentation and Solution Preparation. SEM (JSM 5910, JEOL Japan) and TEM for analyzing the surface morphology of CDGs, EDX (JSM-6390 LV) for elemental composition, FTIR (PerkinElmer) for surface identification of the functional groups and their investigation, a spectrofluorometer (RF-5301, Shimadzu, Japan) equipped with a quartz cell having excitation and emission slit width of 5 nm for fluorescence measurement, and an analogue pH meter (model PHS-3BW 2908 N Chicago) for pH measurement were used.

Stock solutions (100 μg mL^{-1}) of mesotrione, cobalt(II) chloride, and glucose-containing carbon dots (CDG) were prepared in HPLC-grade. Britton Robinson buffer (BRB) solutions of different pH were prepared and used for pH adjustment.

2.3. Synthesis of Glucose-Containing Carbon Dots. The fluorescent active carbon dots were synthesized by adopting sophisticated changes in the basic hydrothermal method following the bottom-up approach.[62] In the initial step, glucose (0.8 g) and ethylenediamine (1.39 mL) were dissolved in distilled water (30 mL). The reagent mixture was placed in a Teflon-lined autoclave and kept in a gas chromatographic oven at a temperature of 120 °C for 8 h. The resultant brownish color product was dried for 2−3 days at 140 °C in a GC oven. The dried product was subsequently dispersed in ethanol (20 mL) and subjected to sonication for 30 min, followed by centrifugation for 20 min at a rate of 12,000 rpm. After filtration, the sample was dried at 60 °C overnight. The final product was obtained in the form of brownish/black color

https://doi.org/10.1021/acsomega.3c07171
ACS Omega 2023, 8, 49115−49128

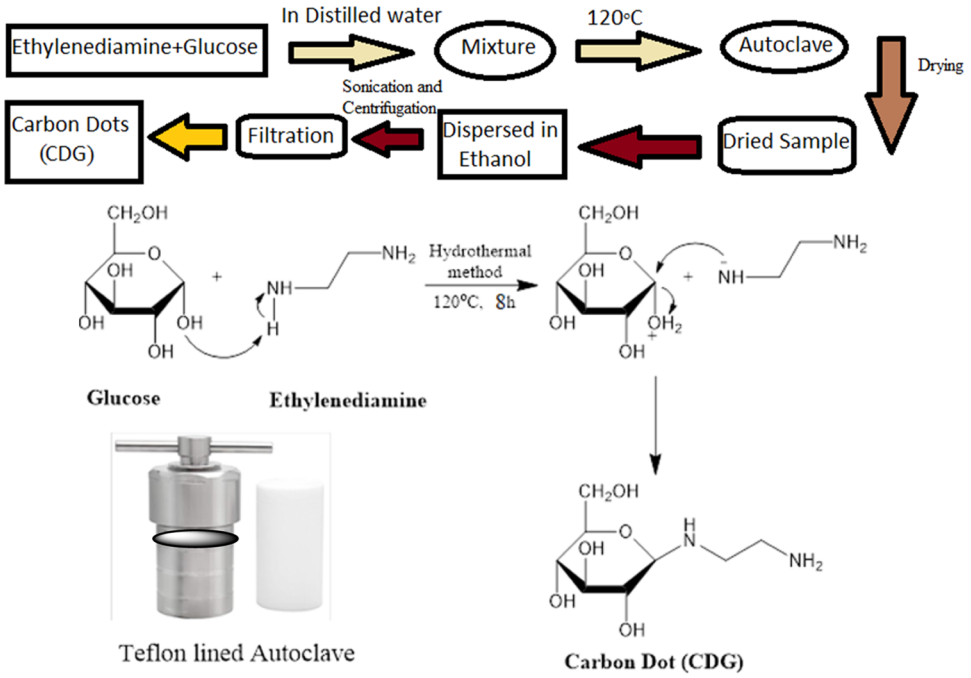

Figure 1. Schematic representation (upper scheme) and synthetic reaction mechanism (lower scheme) for the synthesis of CDGs along with the image of the Teflon-lined autoclave.

CDGs. The synthesis procedure of CDGs is represented in Figure 1.

2.3.1. Measurement of Quantum Yield. The quantum yield (%) of fluorescent CDGs was investigated using quinine sulfate as the selected standard reference. Quinine sulfate, with a known literature quantum yield of 0.54, was dissolved in a 0.1 M H_2SO_4 solution. Meanwhile, the CDG samples were dissolved in distilled water.

2.4. Mesotrione Sensing through CDGs. A series of volumetric flasks of 10 mL each were taken. To get 30 μg mL^{-1} (CDG) and 15 μg mL^{-1} (Co−II), 3.0 mL of CDG solution (100 μg mL^{-1}) and 1.5 mL of Co (II) solution (100 μg mL^{-1}) were mixed. The effect of mesotrione on the fluorescence intensity of the CDGs was investigated by taking different volumes of the mesotrione solution (0.2−5.0 mL) each from the 10 μg mL^{-1} and 100 μg mL^{-1} solutions into separate volumetric flasks. The mesotrione concentrations in the range of 0.2−5.0 μg mL^{-1} were achieved. Subsequently, the FI of each solution was measured against the reagent blank at λ_{em} = 456 nm following excitation at λ_{ex} = 375 nm. The solution of CDG-Co(II) exhibited a pale-yellow color, while the fluorescent color was blue when checked under emission excitation inside the spectrofluorometer, where the different color images are given in Figure S1.

2.5. Analysis of Interference Effects. A comprehensive investigation was conducted using a series of 10 mL volumetric flasks. 0.1 mL of mesotrione solution having a concentration of 10 μg mL^{-1} was added to each flask. Different pesticides having concentrations of 100 μg mL^{-1} were added into the flasks. The optimized concentrations of Co(II) and CDGs were added to each flask. Fluorescence intensity measurements were carried out against their respective blanks. To explore the effect of metal ions, a similar approach was adopted. 0.1 mL of the MST solution (10 μg mL^{-1}) and 3.0 mL of CDG solution (100 μg mL^{-1}) were added to the 10 mL volumetric flasks. Metal ions were added into the flasks in concentrations ranging from 0.2 to 0.6 mL. The FI was recorded against reagent blanks for all the samples.

2.6. Sample Collection/Preparation. To demonstrate the practical applicability of the CDGs as a sensor for mesotrione in various environmental samples, spiking and recovery studies were conducted. The water samples were collected from rivers, lakes, and drinking water sources as well as soil and tomato samples collected from crop fields where the mesotrione was not used. All of the samples were thoroughly cleaned.

Triplicate sets of each sample (5−15 g for soil and tomato samples and 2−6 mL for water samples) were taken and spiked with standard mesotrione solutions to achieve concentrations of 2.0, 4.0, and 6.0 μg g^{-1} for the soil and tomato samples and 0.1, 0.3, and 0.5 μg mL^{-1} for the water samples. Respective blanks for each sample type were prepared. For the facilitation of equilibration, 20 mL of distilled water was added to each mixture, and all samples were allowed to stand in position for 1 h prior to extraction.

2.7. Extraction of Mesotrione. After the spiking and equilibration process, each sample was filtered and 2.0 mL of the filtrate from each sample was taken in separate flasks of 10 mL capacity. 30 μg mL^{-1} of CDG solution, 15 μg mL^{-1} of Co(II) solutions, and BR buffer were added to each flask. The fluorescence intensity of each solution was recorded against the respective sample blank. Appropriate volumes of tomato and soil samples were taken in beakers. 30 μg mL^{-1} of the CDG solution, 15 μg mL^{-1} of Co (II) solutions, and 0.1 μg mL^{-1} of mesotrione solution were added to each beaker and diluted with distilled water. The FI was measured in each case against the blank, and the concentrations of mesotrione and percentage recovery were calculated for each sample.

2.8. Selectivity toward Mesotrione (MST). The sensing approach was extended to determine other mesotrione family herbicides including sulcotrione, tembotrione, and benzofenap in tomato samples. The same procedure for the tomato sample

https://doi.org/10.1021/acsomega.3c07171
ACS Omega 2023, 8, 49115−49128

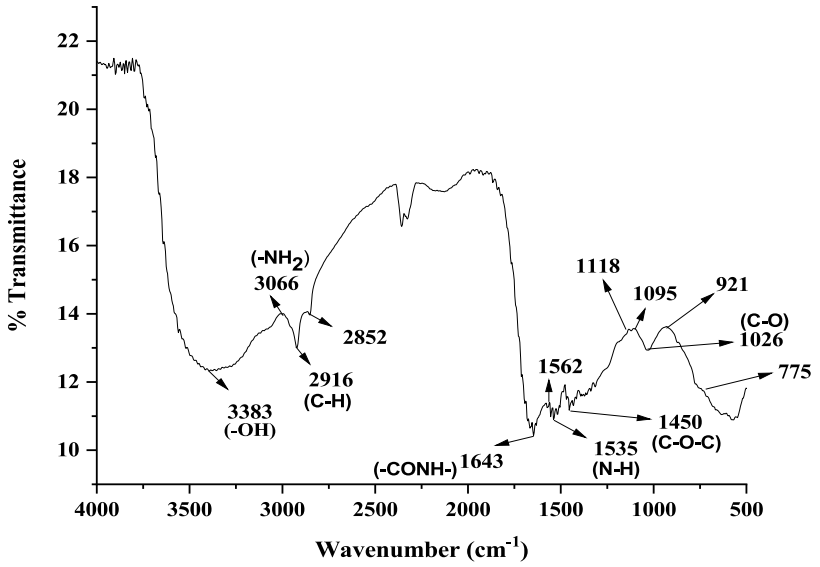

Figure 2. FTIR spectrum of glucose-containing carbon dots.

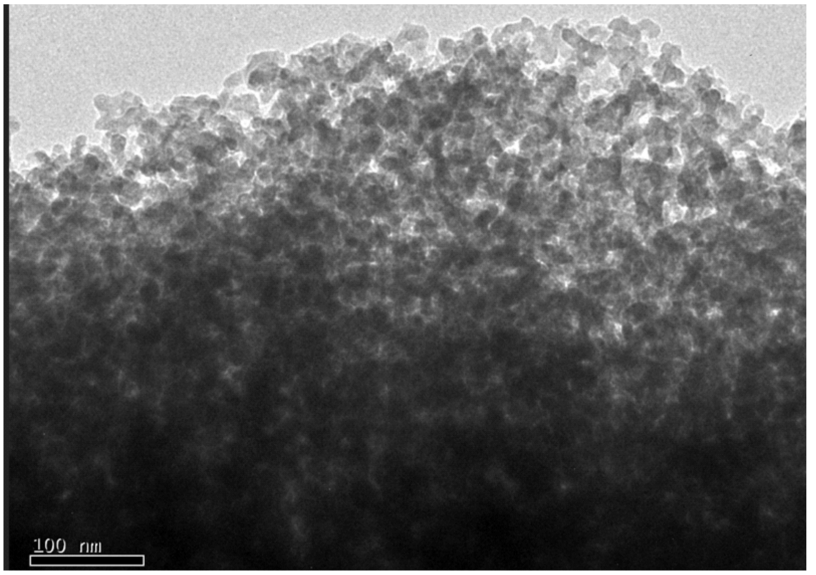

Figure 3. TEM image of glucose-containing carbon dots.

was repeated after spiking with sulcotrione, tembotrione, and benzofenap, and the fluorescence intensity (FI) was detected in each case.

3. RESULTS AND DISCUSSION

3.1. Characterization. *3.1.1. Fourier Transform Infrared Spectrum of the CDGs.* The FTIR spectrum (Figure 2) depicts the successful synthesis of the CDGs containing the corresponding functional groups of reacting moieties. The characteristic band observed at 3066.81 cm^{-1} indicates the presence of an amino (−NH2) group, while the broad peaks at 3383.14 and 1095.56 cm^{-1} are attributed to the stretching vibrational mode of the hydroxyl functional group (O−H) located on the CDG surface. The shoulder peaks at 2852.34, 2916.36, 1562.34, and 1118.71 cm^{-1} are attributed to the stretching vibration of the C−H bonds. Moreover, bands at 1450.46 and 921.97−1026.13 cm^{-1} correspond to vibrations of C−O−C and C−O bonds, respectively. The sharp peak at 1643.35 cm^{-1} is associated with the amide linkage (−CONH−), indicating the presence of ethylenediamine coated at the surface of the carbon dots through the amide group −CONH- linkages. The band observed at 1535.33 cm^{-1} corresponds to the bending vibrations of N−H. Furthermore, bands at 775.38 cm^{-1} correspond to the wagging vibrations of $N-H_2$. Overall, the FTIR findings convincingly confirm the presence of amino and hydroxyl groups originated from ethylenediamine and glucose, respectively.

3.1.2. Morphological Analysis of the CDG via TEM Imaging. Morphological appearance of the carbon dot is visualized in the form of TEM images (Figure 3), which clearly shows that particles are irregular in shape and dimensions. The shape diversity of the particles ranges from spherical through oval to bent structures. The extent of agglomeration of the CDG is clear from the low-resolution TEM image showing the overcrowded nature of the GDG. The TEM images clearly indicated that the CDG particles are in the range of 1 nm, which satisfies the definition of carbon dots. The CDG surface

https://doi.org/10.1021/acsomega.3c07171
ACS Omega 2023, 8, 49115−49128

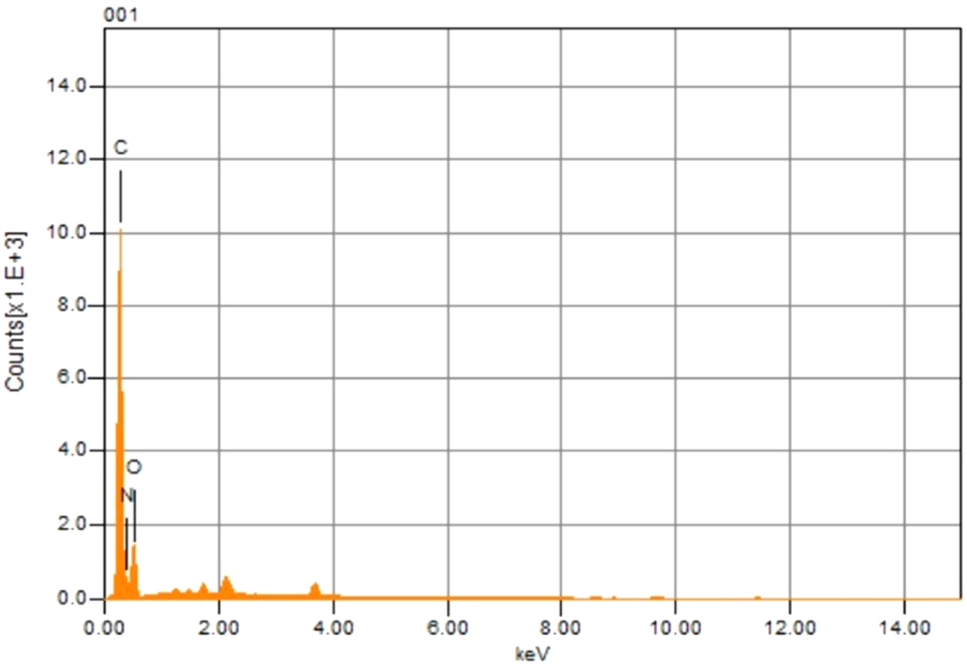

Formula	mass%	Atom%	Sigma	Net	K ratio	Line
C	64.76	70.64	0.03	258463	0.0465058	K
N	4.27	3.99	0.02	18657	0.0455419	K
O	30.97	25.37	0.12	36026	0.0296220	K
Total	100.00	100.00				

Figure 4. EDX plot of the carbon dots.

exhibits some fused pores of quite a small size, which likely contribute to an increased surface area of the CDG.

3.1.3. Energy-Dispersive X-ray (EDX). The elemental composition and atomic ratios of C, O, and N in the CDG were estimated from the EDX spectrum. The EDX spectrum revealed the presence of various elements, with carbon being the most abundant. The percentage composition of C, O, and N in the CDG was estimated to be 70.64, 25.37, and 3.99%, respectively, as illustrated in Figure 4.

3.1.4. Emission Spectra of Carbon Dots (CDGs) at Different Excitation Wavelengths. The maximum fluorescence intensity (FI) for CDGs was detected at 456 nm under excitation at 375 nm. Moreover, the aqueous CDG solution manifested strong blue fluorescence upon excitation at 375 nm. In the case of CDGs, the emission wavelengths displayed a broad spectrum dependent on the excitation wavelengths applied. Notably, when excited at 10 nm interval increments in the range of 355−405 nm, the fluorescence spectra exhibited visual variations, as graphically depicted in Figure 5.

3.1.5. UV−Visible Spectroscopy. The optical characteristics of carbon dots (CDG) were investigated through UV−visible spectroscopy, as shown in Figure 6 (on the left side). This analysis revealed distinct absorption peaks at 224 and 330 nm, attributed to the presence of surface functional states. Another broad low-intensity peak is seen at about 280 nm, which could be caused by the existence of the n-σ^* signal, which indicates the presence of the −OH group. The peak observed at 330 nm can be attributed to the transitions, which may arise from the existence of C−N or C−O functional groups associated with the CDG framework.

3.1.6. Particle Size Distribution Analysis of the CDG. The volume-based particle size of the CDG was determined

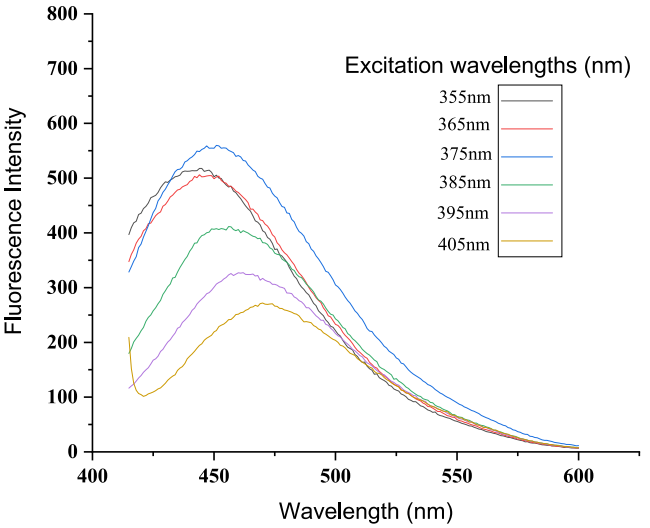

Figure 5. Emission of CDG at different excitation wavelengths.

through master sizers (Figure 6) on the right side. The particle size of CDG is in the range of 1 nm. The particle size distribution data agree with the results of TEM imaging.

3.2. Turn on Fluorescence Sensing of Mesotrione using the CDG. The FI response of the CDG-Co (II) sensor to mesotrione was thoroughly investigated, which is given in Figure 7 (upper plot). As the concentration of mesotrione increased, a significant enhancement in fluorescence intensity was observed at λ_{em} = 456 nm using λ_{ex} at 375 nm. The optimized conditions resulted in the FI enhancement of CDF-Co (II) toward mesotrione clearly showing a linear relation-

https://doi.org/10.1021/acsomega.3c07171
ACS Omega 2023, 8, 49115−49128

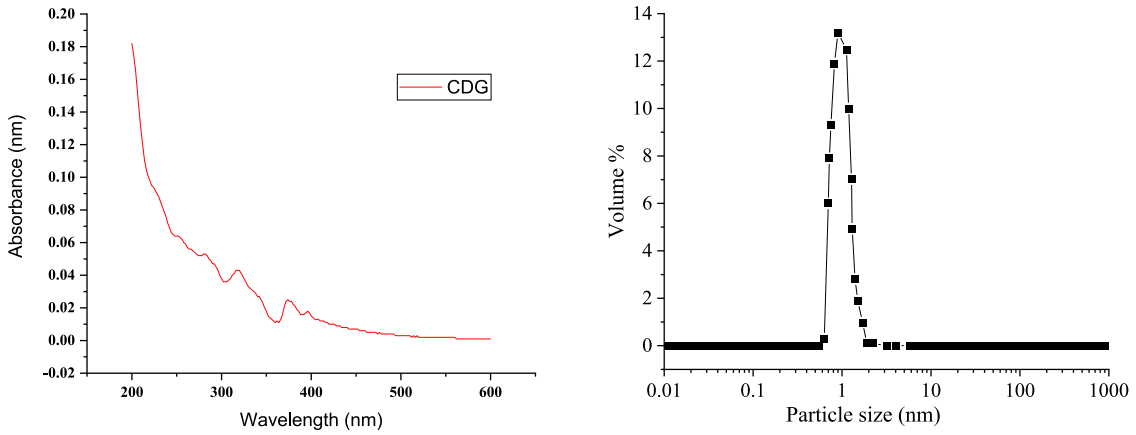

Figure 6. UV−visible absorption spectra of the CDG (on the left) and particle size distribution (on the right).

ship with concentration in the range of 0.2−5.0 μg mL^{-1} where the coefficient of determination (R^2) was 0.9988, as given in Figure 7 (lower plot). Both the fluorescence ON and OFF spectra have been distinctly separated for improved clarity, and comprehensibility is given in Figure 7 (middle plot). In both cases of CDG and CDG-Co(II) Stokes shift occurs; in this shift, the emission (fluorescence) occurs at a longer wavelength (lower energy) at λem = 456 nm, compared to the excitation λex at 375 nm. This indicates that energy is lost during the relaxation process of excited electrons, typically due to vibrational and rotational transitions. The experimental results demonstrated the potential of the CDG-Co (II) as an effective sensing tool for mesotrione detection. The linear increase in FI response with increasing mesotrione concentration makes the proposed method very effective for mesotrione detection and determination. The higher coefficient of determination (R^2) value validates the reliability of the sensor's response, suggesting its suitability for practical applications in the quantification of mesotrione in various environmental samples.

3.3. Batch Analysis: Spectrofluorometric Determination of Mesotrione. *3.3.1. Effect of CDG and Co (II) Concentrations on FI.* Different concentrations of CDG solutions (5.0−40.0 μg mL^{-1}) were mixed with a fixed concentration of Co (II) solution (5.0 μg mL^{-1}) and mesotrione (0.1 μg mL^{-1}). The FI was measured and analyzed in response to varying CDG concentrations. The results shown in Figure 8a show a gradual increase in the FI with increasing CDG concentration up to 30 μg mL^{-1}. However, the FI decreased when checked beyond 30 μg mL^{-1}. So, 30 μg mL^{-1} of the CDG solution was used as the standard for further analysis.

Optimization of the Co (II) concentration at ambient temperature (Figure 8b) was carried out. A gradual increase of the Co (II) concentration (from 5 to 30 μg mL^{-1}) into the aqueous solution of a fixed/optimized concentration of the CDG (30 μg mL^{-1}) resulted in the immediate decrease in the emission peak at 456 nm. The differential quenching effect of Co (II) might be attributed to its electronic nature. The presence of unsaturated electronic states in Co (II) facilitates nonradiative energy/charge transfer from CDG to Co (II), resulting in the formation of a Co (II) complex at the surface of the CDG.[63]

3.3.2. pH and Time Effect on FI. pH of the sensing media plays a critical role during mesotrione detection. FI of the CDG-Co (II) sensor was enhanced by increasing the pH of the medium, reaching its maximum at pH 8. However, the FI demolished gradually beyond pH 8 (Figure 8c). A strong peak was observed in the pH range of 2−8. This behavior might be attributed to the p-p* and n-p* electronic transitions, which are influenced by the filling or depleting of valence bands with pH variations. Under acidic conditions, the groups present at the surface of CDG-Co (II) become protonated, enabling them to coordinate with mesotrione. However, above pH 8, the FI was decreased, which could be attributed to the deprotonation process of the $-NH_2$ and $-OH$ groups at the CDG surface. As the fluorescence signal of the CDG remains stable from pH 2−8, pH 8 was selected as the optimum pH.

As a result of time optimization, FI of the CDG-Co (II) probe for mesotrione detection remains stable up to 75 min (Figure 8d), while the FI decreased slightly when the time exceeded 75 min.

3.3.3. Effect of Different Concentrations of NaCl and Various Solvents. Experiments were conducted utilizing varying concentrations of NaCl and various solvents. Remarkably, the introduction of various NaCl solution concentrations yielded negligible alterations in the experimental outcome (Figure 8e). The observed fluorescence intensity remained consistently stable across a spectrum of ionic strengths, as depicted in this result. Consequently, it is apparent that further experiments involving NaCl are unnecessary. Notably, the data demonstrates a pronounced increase in the CDG reaction's efficacy when dispersing in water, in contrast to other solvents, as illustrated in Figure 8f.

3.4. Sensing Mechanism. The exact mechanism underlying the fluorescence nature of carbon dots remains a subject of ongoing research, as reported by Tafreshi et al.[1] The CDG surface containing hydroxyl groups and basic amine exhibits fluorescence generated through surface-trapped states and electron hole recombination pathways. The electrons are excited to higher energy levels on excitation at 375 nm, resulting in the fluorescence of a beautiful blue color. Due to their low cost and biocompatibility, CDGs have the potential to be integrated with optical analytical equipment to detect drugs, biomolecules, and pesticides using a variety of sensing techniques.[64] In chemical sensing, changes in the CDG fluorescence are monitored in the presence of an analyte. Different heteroatoms are present at the CDG surface, which can potentially enhance sensing phenomena, making it tailored to interact with specific analytes. Fluorescence quenching mechanisms can generally be categorized as static quenching, dynamic quenching, or a combination of the two. The annihilation mechanism is associated with either a single

https://doi.org/10.1021/acsomega.3c07171
ACS Omega 2023, 8, 49115−49128

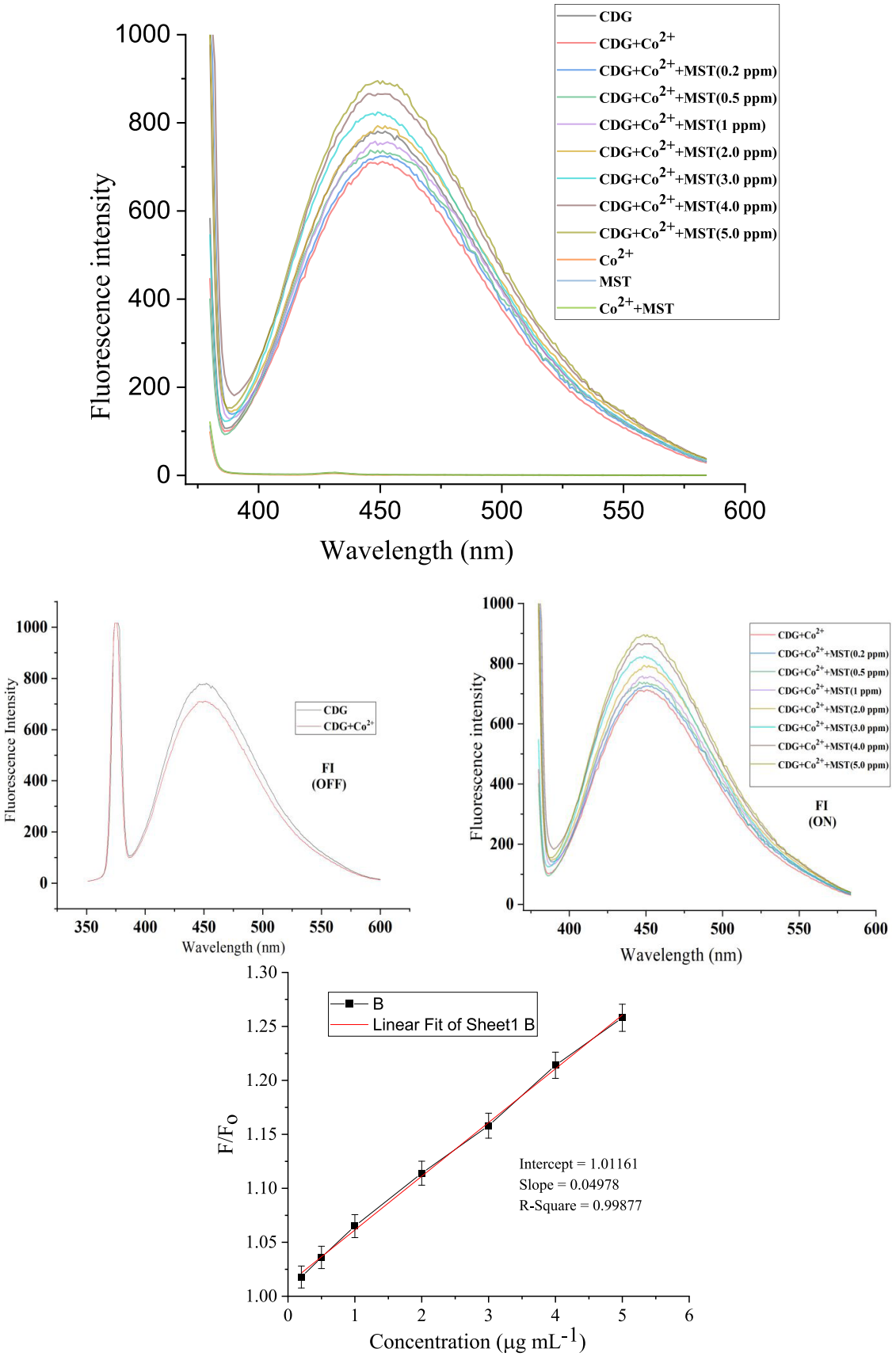

Figure 7. Effect of mesotrione concentration on the fluorescence intensity of the carbon dots (upper plot), the FI-OFF (upper right), and the FI-ON (upper left) spectra. Linear range of FI in the presence of different concentrations of mesotrione (lower plot).

https://doi.org/10.1021/acsomega.3c07171
ACS Omega 2023, 8, 49115−49128

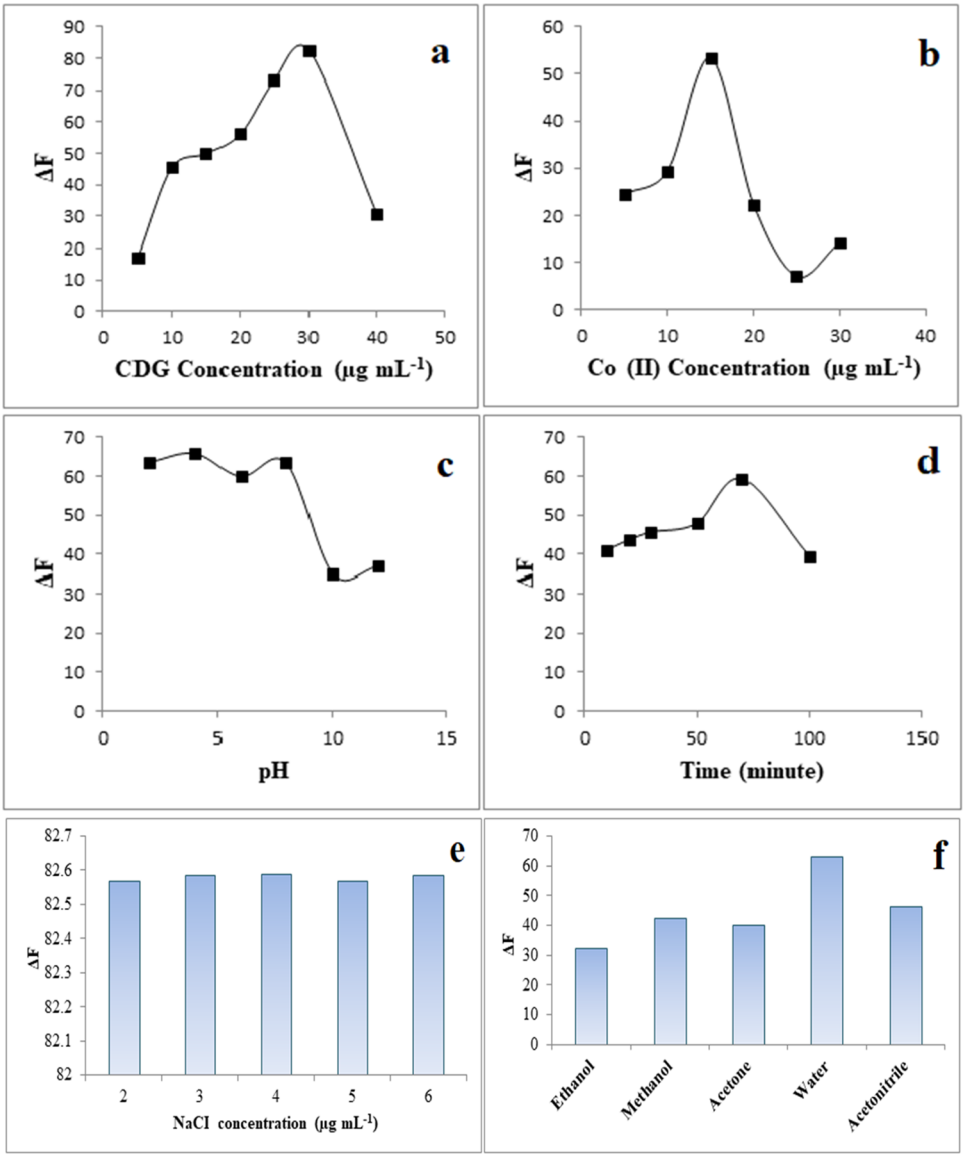

Figure 8. Concentration effect of CDG (a) and Co (II) (b), effect of pH (c) time, (d) NaCl (e), and effect of various solvents (f) on FI.

dynamic or static quenching process when the fluorescence intensity increased linearly with the quencher concentration (Q).[14] Carbon dots of the current project show higher selectivity toward Co (II) due to the presence of OH and NH_2 at the CDG surface, which allows for rapid chelation with Co (II), demonstrating a static fluorescence quenching resulting from the formation of a nonradiative complex between CDG and Co (II). The strong effect of Co(II) fluorescence quenching indicated the CDG's high selectivity for Co (II) over other metals.[65,66] The quenching effect may also be attributed to the transfer of charge between CDG and Co (II) ions.[2]

CDG-based sensing offers a unique approach compared with traditional methods. A comprehensive understanding of the chemical, physical, and optical behaviors of the CDG can lead to improved detection limits of the synthesized CDs.[65] To locate the specific CDG functional groups actively participating in the interaction with target analyte/mesotrione is very challenging and is not always straightforward. However, it is quite genuine that mesotrione selectively interacts with NH_2 and OH groups located at the CDG surface. Mesotrione might undergo either hydrogen bonding, ionic interactions, or covalent binding with the functional groups present at the surface of CDG-Co (II), resulting in the fluorescence enhancement of CDG-Co (II). The interactions between mesotrione and CDG-Co (II) are mainly driven by ground-state complex formation through amino and hydroxyl groups with minor involvement of a dynamic electron transfer reaction.[66] As a result, the precursor of the probe with intense fluorescence is created from the nonfluorescent probe with the photoinduced electron transfer mechanism.[45] The mesotrione determination via fluorescence sensing was successfully established because of the "off−on" strategy.[67,68] The fluorescence efficiency (ΔF) was calculated using the equation $\Delta F = F_0 - F$, where F_0 and F are the fluorescence intensities recorded at 456 nm in the absence and presence of mesotrione in the detection system, respectively.[13,25,26] The schematic representation of the sensing mechanism is illustrated in Figure 9.

3.5. Selectivity. Fluorescence response of the CDG-Co(II) sensor toward mesotrione was investigated in the presence of pesticides (carbofuran, pirimicarb, chlortoluron, imidacloprid,

https://doi.org/10.1021/acsomega.3c07171
ACS Omega 2023, 8, 49115−49128

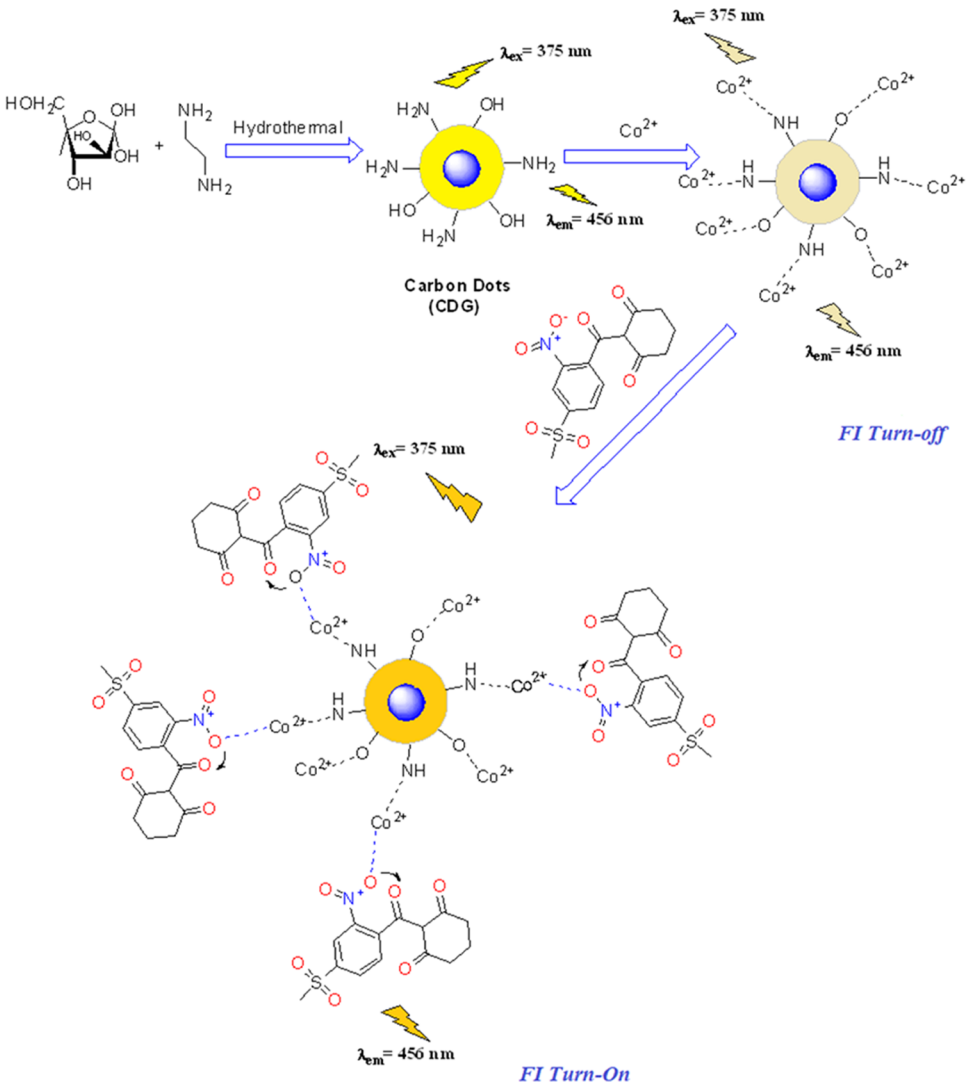

Figure 9. Schematic representation of the mesotrione-sensing mechanism via CDGs.

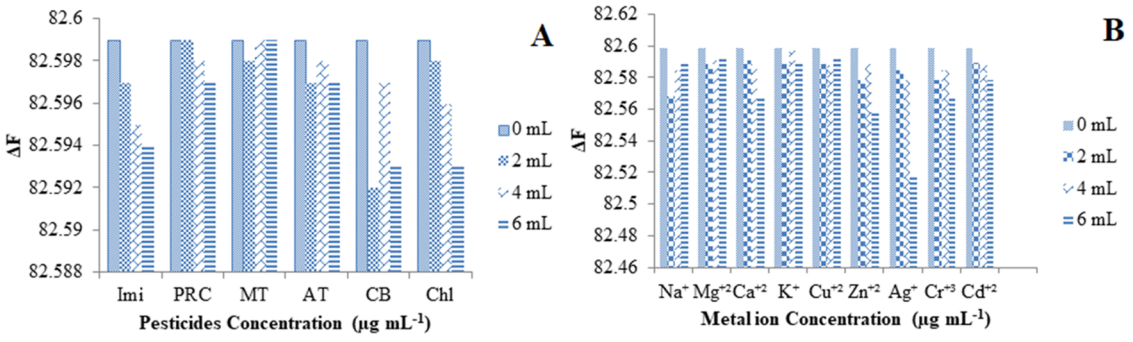

Figure 10. FI response of the CDG-Co(II) sensor toward mesotrione in the presence of other pesticides (A) and metal ions (B).

methomyl, and atrazine) and metal ions (Ca^{2+}, Na^{+}, Mg^{2+}, Cu^{+}, K^{+}, Zn^{2+}, Ag^{+}, Cr^{3+}, and Cd^{2+}). Enhancement in the FI of CDG with mesotrione was significantly higher than that with other pesticides (Figure 10A). Similarly, the FI response of the CDG toward mesotrione was much higher in the presence of Co(II) compared to other metal ions (Figure 10B), demonstrating insignificant interference effect from similar types of metals in the sensing phenomenon.

3.6. Stability of the CDG. The physical and chemical stabilities of carbon dots are very important for their practical applications. The carbon dots synthesized in the current project were monitored regularly right after their synthesis at time intervals of three months, five months, seven months, and one year. FI of the CDG remained very stable throughout these intervals since the emission intensity at 456 nm was nearly unchanged (Figure 11). The carbon dots exhibited very good thermal, mechanical, and chemical stability over extended

https://doi.org/10.1021/acsomega.3c07171
ACS Omega 2023, 8, 49115−49128

Table 1. Analytical Results for Mesotrione Determination in Different Samples using the CDGs

sample	mass of sample (g), mL	mass of MST added (μg)	F/F_o	concentration found (μg mL^{-1})	mass of MST found (μg)	percent recovery	average % recovery ± SD
tomato sample	5	20	1.0125	0.019	19.8	99.39	99.73 ± 0.57
		40	1.0136	0.040	40.1	100.40	
		60	1.0145	0.059	59.6	99.39	
	10	20	1.0125	0.019	19.0	95.38	98.44 ± 2.65
		40	1.0135	0.039	39.9	99.89	
		60	1.0145	0.060	60.0	100.06	
	15	20	1.0126	0.020	20.6	103.41	102.52 ± 2.46
		40	1.0136	0.041	41.7	104.41	
		60	1.0145	0.059	59.8	99.73	
soil sample	5	20	1.0217	0.203	20.3	101.70	101.00 ± 0.61
		40	1.0316	0.402	40.2	100.55	
		60	1.0417	0.604	60.4	100.76	
	10	20	1.0217	0.204	20.4	102.10	100.77 ± 1.49
		40	1.0317	0.404	40.4	101.05	
		60	1.0412	0.594	59.4	99.16	
	15	20	1.0220	0.209	20.9	104.71	103.28 ± 1.89
		40	1.0323	0.415	41.5	103.96	
		60	1.0418	0.607	60.7	101.17	
river water	2	1	1.0165	0.099	0.99	99.59	100.04 ± 0.66
		3	1.0265	0.299	2.99	99.73	
		5	1.0367	0.504	5.04	100.80	
	4	1	1.0164	0.098	0.98	98.19	99.14 ± 2.56
		3	1.0266	0.301	3.01	100.53	
		5	1.0366	0.503	5.03	100.72	
	6	1	1.0163	0.096	0.96	96.18	96.18 ± 2.58
		3	1.0265	0.299	2.99	99.79	
		5	1.0368	0.506	5.06	101.20	
lake water	2	1	1.0166	0.100	1.00	100.40	100.66 ± 0.46
		3	1.0266	0.301	3.01	100.40	
		5	1.0368	0.506	5.06	101.20	
	4	1	1.0164	0.096	0.96	96.38	98.39 ± 2.01
		3	1.0266	0.301	3.01	100.40	
		5	1.0361	0.491	4.91	98.39	
	6	1	1.0164	0.096	0.96	96.38	96.38 ± 2.22
		3	1.0264	0.297	2.97	99.06	
		5	1.0367	0.504	5.04	100.80	
drinking water	2	1	1.0166	0.100	1.00	100.40	100.53 ± 0.23
		3	1.0266	0.301	3.01	100.40	
		5	1.0367	0.504	5.04	100.80	
	4	1	1.0166	0.100	1.00	100.40	98.83 ± 2.15
		3	1.0265	0.299	2.99	99.73	
		5	1.0366	0.502	5.02	100.40	
	6	1	1.0164	0.096	0.96	96.38	96.38 ± 1.61
		3	1.0262	0.293	2.93	97.72	
		5	1.0364	0.497	4.97	99.59	

periods of time, ensuring their reliability and usefulness in practical applications. Furthermore, no visual discoloration or detrimental photobleaching was observed. The CDG showed stability under acidic and neutral media where a slight decrease in the FI was observed at higher pH.

3.7. Application of the Proposed Method to Real Sample Analysis. To assess the feasibility, efficacy, and efficiency of the proposed sensor in real sample applications, the sensing approach was extended to determine mesotrione in various environmental samples, including water samples from rivers, lakes, and drinking sources, as well as soil and tomato samples. The results demonstrated the highest recovery percentage in all cases, confirming the applicability of the proposed method. As summarized in Table 1, the range of recovery fell within 95.38−104.7%, indicating the reasonable accuracy and reproducibility of the fluorescence sensor. Consequently, it can be effectively employed for the detection of mesotrione in real samples.

3.7.1. Selectivity toward Mesotrione (MST). The sensing approach of the newly proposed Co (II)-integrated carbon dots was extended to determine other members of the triketone class of pesticides, such as sulcotrione, tembotrione, and benzofenap, in tomato samples. The results showed the highest percentage recovery of mesotrione, and a very small fluorescence enhancement was observed for sulcotrione, tembotrione, and benzofenap. Among the pesticides other than mesotrione, the highest recovery of 20% was recorded for sulcotrione due to its structural similarity to mesotrione. The

https://doi.org/10.1021/acsomega.3c07171
ACS Omega 2023, 8, 49115−49128

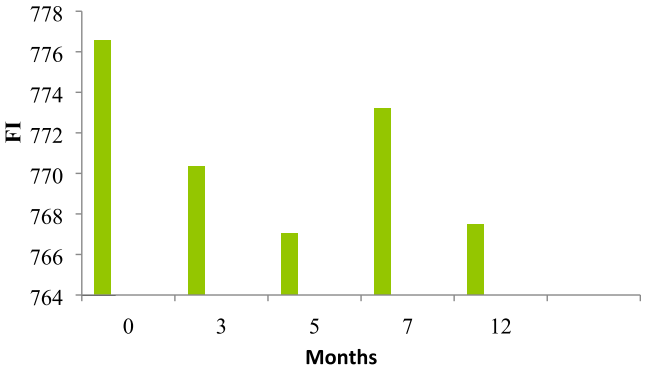

Figure 11. Stability of carbon dots (CDGs).

Table 2. Selectivity toward Mesotrione Determination in the Presence of Other Triketone Pesticides in the Tomato Sample using the CDGs

name of pesticide	spiking amount of pesticides (μg)	F/F_o	conc found (μg mL^{-1})	mass of pesticides found (μg)	percent recovery
mesotrione	40	1.0136	0.04	40.16	100.40
sulcotrione	40	1.0120	0.008	8.032	20.08
tembotrione	40	1.0118	0.004	4.016	10.040
benzofenap	40	1.0117	0.002	3.008	7.52

Mass of the tomato sample was 5 g in each case.

Table 3. Analytical Figures of Merit

title	value
λ_{exi} (nm)	375 nm
λ_{emi} (nm)	456 nm
linear range (μg mL^{-1})	(0.2−5.0 μg mL^{-1})
slope	0.0498
intercept	1.0116
regression equation	0.0498x + 1.0116
regression coefficient (R^2)	0.9988
standard deviation (SD) (μg mL^{-1})	0.00082 μg mL^{-1}
relative standard deviation (RSD) (%)	0.682%
LOD (μg mL^{-1})	0.054 μg mL^{-1}
LOQ (μg mL^{-1})	0.164 μg mL^{-1}

overall results, which are briefly summarized in Table 2, confirm the applicability of the proposed method with very good accuracy of the proposed fluorescence sensor.

3.8. Analytical Figures of Merit. Under the optimum experimental conditions, the calibration curve exhibited a linear response over the concentration range 0.2−5.0 μg mL^{-1}. Parameters of the calibration curve including the linear range, intercept, slope, regression equation, regression coefficient, standard deviation, limit of detection, and relative standard deviation are summarized in Table 3.

3.9. Comparison of Modifications in Hydrothermal Protocols Reported for the Synthesis of Carbon Dots. Different research groups renovated the basic hydrothermal protocol for the synthesis of carbon dots in terms of reaction time, solvent media, and temperature; the summary is given in Table 4. In the current study, various batches of carbon dots were synthesized each time making some changes in the hydrothermal method. Finally, a set of parameters was optimized, which successfully resulted in the synthesis of carbon dots. Besides those changes, we used a Teflon-lined autoclave instead of the traditional autoclave, which is time effective and very easy in operation. We expect very good yield of the carbon dots in the current study, and the carbon dots are not agglomerated, which can be seen form the TEM image. The protocol and method used in the current study seems better than the reported methods, making it a better choice for carbon dot synthesis.

3.10. Comparative Analysis of the Currently Proposed and Reported Methods. Limited methods have been reported for the determination of mesotrione. A thorough comparison of the results obtained in the current study with those of the reported literature being summarized in Table 5 supports the superiority of the sensing probe designed in the current study. The parameters selected for comparison are percentage recovery, determination coefficient (R^2), limit of detection, limit of quantification, % relative standard deviation, and linear range.[49,53−5455565758596061]

4. CONCLUSIONS

A facile and cost-effective procedure for the direct synthesis of Co(II)-integrated glucose-bound carbon dots was proposed by incorporating simple modifications in the hydrothermal process. A simple Teflon-lined autoclave was used instead of the traditional autoclave. The carbon dots exhibited strong fluorescence, which was efficiently quenched by the addition of Co (II), owing to the formation of a fluorescent CDG-Co (II) ground-state complex. However, addition of the mesotrione to the system resulted in a reasonable enhancement of the fluorescence intensity due to the strong affinity of mesotrione toward Co (II). Thus, a reliable determination method for the mesotrione was established with improved characteristics such as specificity, accuracy, sensitivity, precision, acceptable recovery, and a wide linear range. The fast, simple, and cost-effective nature of the compound makes it an attractive option for practical applications. The proposed sensing system is a promising approach for the detection of mesotrione traces in real environmental and agricultural samples. The current study not only contributes to the advancement of nanomaterial-

Table 4. Comparison of Parameters/Steps Used in the Hydrothermal Method Practiced by Different Research Groups

precursors	time (h)	solvent	temperature (°C)	quantum yield (%)	references
feather	7	H_2O_2, NH_3	160		29
3-aminobenzeneboronic acid	12	H_2O	180		31
L-arginine	14	H_2O	240		44
3-aminophenol	12	ethanol, HCl, HNO_3, ethyl acetate, ethanol	140	2.5	69
radish	7	H_2SO_4, NaOH	200		70
P phenenediamine+urea	10	H_2O, ethyl acetate and ethanol	160	35	71
aloe	11	H_2O, dichloromethane	180	10.37	72
glucose + ethylendiamine	8	H_2O	120	22	current study

https://doi.org/10.1021/acsomega.3c07171
ACS Omega 2023, 8, 49115−49128

Table 5. Comparison of the Proposed Method to the Methods Reported in the Literature for the Determination of Mesotrione

method/technique	% recovery	R^2	LOD (μg mL^{-1})	LOQ (μg mL^{-1})	linear range (μg mL^{-1})	% RSD	reference
fluorescence spectrophotometer	91−96	0.991	0.024		0.076−15	3.2−6.1	ref14
fluorescence spectrometer	101−105, 96−109, 98−117	0.996	0.054, 0.14, 1.085			3.2	ref45
Soxhlet extraction (RP-HPLC)	82−97	0.998	0.10	0.35	0.10−5.00	3.7	ref47
square wave voltammetry		0.998	0.088		0.084−16.97		ref48
HPLC	80−97	0.999	0.02		0.5−5.0		ref50
cyclic voltammetry	96−99	0.999	0.02		0.03−3.39		ref51
spectrophotometric	95−106.5	0.991	0.053	0.162	0.2−10	0.276	ref52
solid-phase extraction	89	0.997	0.02	60	1.50−100		ref66
spectrofluorimetry	95−104.7	0.999	0.054	0.164	0.2−5.0	0.682	current study

based sensing technology but also addresses the pressing needs for efficient detection methods of mesotrione.

■ ASSOCIATED CONTENT

Supporting Information

The Supporting Information is available free of charge at https://pubs.acs.org/doi/10.1021/acsomega.3c07171.

It includes two additional tables, Table S1 and S2, and a photographic image of the CDG in a spectrofluorometer and CDG solution in Figure S1 (PDF)

■ AUTHOR INFORMATION

Corresponding Author

Faiz Ali − *Department of Chemistry, University of Malakand, Chakdara 18800 Khyber Pakhtunkhwa, Pakistan;* orcid.org/0000-0002-4984-164X; Email: faizy186@gmail.com

Authors

Rani − *Department of Chemistry, University of Malakand, Chakdara 18800 Khyber Pakhtunkhwa, Pakistan*

Mian Muhammad − *Department of Chemistry, University of Malakand, Chakdara 18800 Khyber Pakhtunkhwa, Pakistan*

Zeid A. AlOthman − *Chemistry Department, College of Science, King Saud University, Riyadh 11451, Saudi Arabia;* orcid.org/0000-0001-9970-2480

Complete contact information is available at: https://pubs.acs.org/10.1021/acsomega.3c07171

Notes

The authors declare no competing financial interest.

■ ACKNOWLEDGMENTS

This research was supported by the University of Malakand through Higher Education Commission (HEC) of Pakistan Project no: 20-14499/NRPU/R&D/HEC/2021. The authors are grateful to the researchers supporting Project No. (RSP2023R1), King Saud University, Riyadh, Saudi Arabia.

■ REFERENCES

(1) Ashrafi Tafreshi, F.; Fatahi, Z.; Ghasemi, S. F.; Taherian, A.; EsfandiariI, N. Ultrasensitive fluorescent detection of pesticides in real sample by using green carbon dots. *PLoS One* **2020**, *15*, No. e0230646.

(2) Deka, M. J.; Dutta, P.; Sarma, S.; Medhi, O. K.; Talukdar, N. C.; Chowdhury, D. Carbon dots derived from water hyacinth and their application as a sensor for pretilachlor. *Heliyon* **2019**, *5*, No. e01985.

(3) Calatayud, J. M.; Ascencao, J. G. d.; Garcıa, J. R. A. FIA-Fluorimetric Determination of the Pesticide 3-Indolyl Acetic Acid. *J. Fluoresc.* **2006**, *16*, 61−67.

(4) Mandal, P.; Sahoo, D.; Sarkar, P.; Chakraborty, K.; Das, S. Fluorescence turn-on and turn-off sensing of pesticides by carbon dot-based sensor. *New. J. Chem.* **2019**, *43*, 12137−12151.

(5) Navarro, M. V.; Cabezon, M. A.; Damiani, P. C. Simultaneous determination of pesticides in fruits by using second-order fluorescence data resolved by unfolded partial least-squares coupled to residual bilinearization. *J. Chem.* **2020**, No. 3217465.

(6) Liu, T.; Su, H.; Qu, X.; Ju, P.; Cui, L.; Ai, S. Acetylcholinesterase biosensor based on 3-carboxyphenylboronic acid/reduced graphene oxide−gold nanocomposites modified electrode for amperometric detection of organophosphorus and carbamate pesticides. *Sens. Actuators, B* **2011**, *160*, 1255−1261.

(7) Zhao, S.; Lei, J.; Huo, D.; Hou, C.; Yang, P.; Huang, J.; Luo, X. A laser-induced fluorescent detector for pesticide residue detection based on the spectral recognition method. *Anal. Methods* **2018**, *10*, 5507−5515.

(8) Flynn, K.; Lothenbach, D.; Whiteman, F.; Hammermeister, D.; Touart, L. W.; Swintek, J.; Johnson, R.; et al. Summary of the development the US Environmental Protection Agency's Medaka Extended One Generation Reproduction Test (MEOGRT) using data from 9 multigenerational medaka tests. *Environ. Toxicol. Chem.* **2017**, *36*, 3387−3403.

(9) Dias, J. V.; Cutillas, V.; Lozano, A.; Pizzutti, I. R.; Fernández-Alba, A. R. Determination of pesticides in edible oils by liquid chromatography-tandem mass spectrometry employing new generation materials for dispersive solid phase extraction clean-up. *J. Chromatogr. A* **2016**, *1462*, 8−18.

(10) Perry, E. D.; Ciliberto, F.; Hennessy, D. A.; Moschini, G. Genetically engineered crops and pesticide use in US maize and soybeans. *Sci. Adv.* **2016**, *2*, No. e1600850.

(11) Alsbaiee, A.; Smith, B. J.; Xiao, L.; Ling, Y.; Helbling, D. E.; Dichtel, W. R. Rapid removal of organic micropollutants from water by a porous β-cyclodextrin polymer. *Nature* **2016**, *529*, 190−194.

(12) Petrarca, M. H.; Fernandes, J. O.; Godoy, H. T.; Cunha, S. C. Multiclass pesticide analysis in fruit-based baby food: A comparative study of sample preparation techniques previous to gas chromatography-mass spectrometry. *Food Chem.* **2016**, *212*, 528−536.

(13) Farajzadeh, M. A.; Bamorowat, M.; Mogaddam, M. R. A. Development of a dispersive liquid-liquid microextraction method based on solidification of a floating ionic liquid for extraction of carbamate pesticides from fruit juice and vegetable samples. *RSC Adv.* **2016**, *6*, 112939−112948.

(14) Sun, X.; Liu, Y.; Niu, N.; Chen, L. Synthesis of molecularly imprinted fluorescent probe based on biomass-derived carbon quantum dots for detection of mesotrione. *Anal. Bioanal. Chem.* **2019**, *411*, 5515−5530.

(15) Mitchell, G.; Bartlett, D. W.; Fraser, T. E.; Hawkes, T. R.; Holt, D. C.; Townson, J. K.; Wichert, R. A. Mesotrione: a new selective herbicide for use in maize. *Pest Manage. Sci.* **2001**, *572*, 120−128.

(16) Felix, J.; Doohana, D. J.; Bruins, D. Differential vegetable crop responses to mesotrione soil residues a year after application. *Crop Prot.* **2007**, *26*, 1395−1403.
(17) Alferness, P.; Wiebe, L. Determination of Mesotrione Residues and Metabolites in Crops, Soil, and Water by Liquid Chromatography with Fluorescence Detection. *J. Agric. Food Chem.* **2002**, *50*, 3926−3934.
(18) Armel, G. R.; Wilson, H. P.; Richardson, R. J.; Hines, T. E. Mesotrione, Acetochlor, and Atrazine for Weed Management in Corn (Zea mays). *Weed Technol.* **2003**, *17*, 284−290.
(19) Panescu, P. H.; Rose, D. A.; Chen, K. K.; Kashanchi, G. N.; Maynard, H. D. Mesotrione Conjugation Strategies to Create Proherbicides with Reduced Soil Mobility. *ACS Sustainable Chem. Eng.* **2021**, *9*, 5776−5782.
(20) Nemes, P.; Kalman, E. Determination of mesotrione in soil and water samples using solid-phase microextraction and gas chromatography-mass spectrometry. *J. Sep. Sci.* **2019**, *42*, 2355−2363.
(21) Li, X.; Li, S.; Li, J.; Zhang, Q.; Yang, Y.; Li, Y. Development of an enzyme-linked immunosorbent assay for the determination of mesotrione in soil and water samples. *Environ. Sci. Pollut. Res.* **2017**, *24*, 20663−20670.
(22) Chahboune, R.; Sarakha, M. Homolytic Scission as the Main Pathway in the Liquid Chromatography/ Electrospray Ionization Quadrupole Time-of-Flight Mass Spectrometry of Mesotrione and its Photoproducts. *Mass Spectrom. Pur. Technol.* **2018**, *04*, No. 125.
(23) Zhang, X.; Zhao, M.; Yang, X.; Liu, Y.; Wang, S. Rapid and sensitive determination of mesotrione in corn, soybean, and soil using high-performance liquid chromatography and liquid chromatography-tandem mass spectrometry. *J. Agric. Food Chem.* **2017**, *65*, 5716−5721.
(24) Tao, H.; Liao, X.; Sun, C.; Xie, X.; Zhong, F.; Yi, Z.; Huang, Y. A carbon dots-CdTe quantum dots fluorescence resonance energy transfer system for the analysis of ultra-trace chlortoluron in water. *Spectrochim. Acta, Part A* **2015**, *136*, 1328−1334.
(25) Muhammad, M.; Jan, M. R.; Shah, J.; Ara, B. Determination of Isoproturon in Environmental Samples using the QuEChERS Extraction-Spectrofluorimetric Method. *Environ. Toxicol. Chem.* **2019**, *38*, 2614−2620.
(26) Songa, E. A.; Okonkwo, J. O. Recent approaches to improving selectivity and sensitivity of enzyme-based biosensors for organophosphorus pesticides: a review. *Talanta* **2016**, *155*, 289−304.
(27) Wei, J.; Yang, Y.; Dong, J.; Wang, S.; Li, P. Fluorometric determination of pesticides and organophosphates using nanoceria as a phosphatase mimic and an inner filter effect on carbon nanodots. *Microchim. Acta.* **2019**, *186*, No. 66.
(28) De, B.; Karak, N. A green and facile approach for the synthesis of water-soluble fluorescent carbon dots from banana juice. *RSC Adv.* **2013**, *3*, 8286−8290.
(29) Hou, J.; Dong, G.; Tian, Z.; Lu, J.; Wang, Q.; Ai, S.; Wang, M. A sensitive fluorescent sensor for selective determination of dichlorvos based on the recovered fluorescence of carbon dots-Cu(II) system. *Food Chem.* **2016**, *202*, 81−87.
(30) Yang, J.; Gao, G.; Zhang, X.; Ma, Y.; Chen, Xi.; Wu, F. One-step synthesized carbon dots with bacterial contact-enhanced fluorescence emission property: Fast Gram-type identification and selective Gram-positive bacterial inactivation. *Carbon* **2019**, *146*, 827−839.
(31) Yan, X.; Song, Y.; Zhu, C.; Li, H.; Du, D.; Su, X.; Lin, Y. MnO_2 Nanosheet-Carbon Dots Sensing Platform for Sensitive Detection of Organophosphorus Pesticides. *Anal. Chem.* **2018**, *90*, 2618−2624.
(32) Liang, W.; Ge, L.; Hou, X.; Ren 1, X.; Yang, L.; Bunker, C. E.; Overton, C. M.; Wang, P.; Sun, Y. Evaluation of Commercial Carbon Quantum Dot Sample on Origins of Red Absorption and Emission Features. *J. Carbon Res.* **2019**, *5* (4), No. 70.
(33) Peng, Z.; Zhou, Y.; Ji, C.; Pardo, J.; Mintz, K. J.; Pandey, R. R.; Chusuei, C. C.; Graham, R. M.; Yan, G.; Leblanc, R. M. Facile Synthesis of "Boron-Doped" Carbon Dots and their Application in Visible-Light-Driven Photocatalytic Degradation of Organic Dyes. *Nanomatererials* **2020**, *1560* (8), No. 1560.
(34) Gogoi, J.; Chowdhury, D. Calcium-modified carbon dots derived from polyethylene glycol: fluorescence-based detection of Trifluralin herbicide, Mater. *Life Sci.* **2020**, *55*, 11597−11608.
(35) Keçili, R.; Hussain, C. G.; Hussain, C. M. Emerging trends in green carbon dots coated with molecularly imprinted polymers for sensor platforms. *TrAC, Trends Anal. Chem.* **2023**, *166*, No. 117205.
(36) Kumar, P. J. V.; Kavitha, G.; Albasher, G.; Sajjad, M.; Arulmozhi, R.; Komal, M.; Nivetha, M. S.; Abirami, N. Multiplex heteroatoms doped carbon nano dots with enhanced catalytic reduction of ionic dyes and QR code security label for anti-spurious applications. *Chemosphere* **2022**, *307*, No. 136003.
(37) Murugan, K.; Kumar Jothi, V.; Rajaram, A.; Natarajan, A. Novel Metal-Free Fluorescent Sensor Based on Molecularly Imprinted Polymer N-CDs@MIP for Highly Selective Detection of TNP. *ACS Omega* **2022**, *7*, 1368−1379.
(38) Rajendran, S.; Zichri, S. B.; Vipinachandran, V. U.; Jelinek, R.; Bhunia, S. K. Triphenylphosphonium-Derived Bright Green Fluorescent Carbon Dots for Mitochondrial Targeting and Rapid Selective Detection of Tetracycline. *ChemNanoMater.* **2021**, *7*, 545−552.
(39) Dolai, S.; Bhunia, S. K.; Rajendran, S.; Ushavipinachandran, V.; Ray, S. C.; Kluson, P. Tunable fluorescent carbon dots: synthesis progress, fluorescence origin, selective and sensitive volatile organic compounds detection. *Crit. Rev. Solid State Mater. Sci.* **2021**, *46*, 349−370.
(40) Chu, H.-W.; Unnikrishnan, B.; Anand, A.; Lin, Y.; Huang, C. Carbon quantum dots for the detection of antibiotics and pesticides. *J. Food Drug Anal.* **2020**, *28*, 539−557.
(41) Rajendran, S.; UshaVipinachandran, V.; Haroon, K. H. B.; Ashokan, I.; Bhunia, S. K. A comprehensive review on multi-colored emissive carbon dots as fluorescent probes for the detection of pharmaceutical drugs in water. *Anal. Methods* **2022**, *14*, 4263−4291.
(42) Ashokan, I.; Bhunia, S. K. Boron and nitrogen co-doped bright yellow fluorescent carbon dots as real-time selective detection of phthalic acid plasticizer in aqueous medium. *J. Photochem. Photobiol., A* **2023**, *437*, No. 114489.
(43) Yen, Y.-T.; Lin, Y.; Chen, T. Y.; Chyueh, S.; Chang, H. Carbon dots functionalized papers for high-throughput sensing of 4-chloroethcathinone and its analogues in crime sites. *Royal. Soc. Chem.* **2019**, *6*, No. 191017.
(44) Liu, L.; Gong, H.; Li, D.; Zhao, L. Synthesis of Carbon Dots from Pear Juice for Fluorescence Detection of Cu^{2+} Ion in Water. *J. Nanosci. Nanotechnol.* **2018**, *18*, 5327−5332.
(45) Liu, Y.; Li, L.; Yue, M.; Yang, L.; Sun, F.; Xu, G.; Fu, Y.; Ye, F. A Switch-On fluorescent probe for detection of mesotrione based on the straightforward cleavage of carbon-nitrogen double bond of Schiff base. *J. Chem. Eng.* **2022**, *430*, No. 132758.
(46) Mastichiadis, C.; Christofidis, I.; Koupparis, M. A.; Willetts, C.; Kakabakos, S. E. Solid-phase fluoroimmunoassay for the determination of mesotrione a novel triketone herbicide in water with direct measurement of the fluorescence onto the solid support. *Analyst* **2003**, *128*, 404−410.
(47) Baranowska, I.; Akdogan, A.; Barchañska, H.; Divrikli, U.; Elci, L. Determination of Mesotrione, Simazine and Atrazine by RP-HPLC in Thermal Water, Sediment and Vegetable Samples. *Anal. Chem. Lett.* **2012**, *2*, 206−219.
(48) Kamga Wagheu, J.; Forano, C.; Hoggan, P. B.; Tonle, I. K.; Ngameni, E.; Mousty, C. Electrochemical determination of mesotrione at organoclay modified glassy carbon electrodes. *Talanta* **2013**, *103*, 337−343.
(49) Dobrzanski, T.; Gravina, F.; Steckling, B.; Olchanheski, L. R.; Sprenger, R. F.; Espírito Santo, B. C.; Santo, B. C. E.; Galvao, C. W.; Reche, P. M.; Prestes, R. A.; Pileggi, S. A. V.; Campos, F. R.; Azevedo, R. A.; Sadowsky, M. J.; Beltrame, F. L. Bacillus megaterium strains derived from water and soil exhibit differential responses to the herbicide mesotrione. *Plos One* **2018**, *13*, No. e0196166.
(50) Barchanska, H.; Rusek, M.; Szatkowska, A. New procedures for simultaneous determination of mesotrione and atrazine in water and soil. Comparison of the degradation processes of mesotrione and atrazine. *Environ. Monit Assess.* **2012**, *184*, 321−334.

https://doi.org/10.1021/acsomega.3c07171
ACS Omega 2023, 8, 49115−49128

(51) Erdodu, G.; Titretir, S. Voltammetric, Determination of Mesotrione at Hanging Mercury Drop Electrode. *J. Anal. Chem.* **2007**, *62* (8), 777−780.
(52) Muhammad, M.; Khan, S.; Fayaz, H. Charge-transfer complex−based spectrophotometric method for the determination of mesotrione in environmental sample. *Environ. Monit Assess.* **2021**, *193*, 681.
(53) Bera, M. K.; Behera, L.; Mohapatra, S. A fluorescence turn-down-up detection of Cu^{2+} and pesticide quinalphos using carbon quantum dot integrated UiO-66-NH2. *Colloids Surf., A* **2021**, *624*, No. 126792.
(54) Muhammad, M.; Ara, B.; Ali, F.; Ahmad, I.; Ullah, H. Mn-Dopped ZnS Quantuum Dots as sensitive sensor for determination of Ciprofloxacin in Pharmaceutical and Biological samples. *J. Chil. Chem. Soc.* **2021**, *66*, 5130−5135.
(55) Katmeh, M. F.; Aherne, G. W.; Stevenson, D. Competitive Enzyme-linked lmmunosorbent Assay for the Determination of the Phenylurea Herbicide Chlortoluron in Water and Biological Fluids. *Analyst* **1996**, *12*, 1699−1703.
(56) Mashuni, M.; Ritonga, H.; Jahiding, M.; Rubak, B.; Hamid, F. H. Highly Sensitive Detection of Carbaryl Pesticides Using Potentiometric Biosensor with Nanocomposite Ag/r-Graphene Oxide/Chitosan Immobilized Acetylcholinesterase Enzyme. *Chemosensors* **2022**, *10* (4), No. 138.
(57) Haddaoui, M.; Raouaf, N. Chlortoluron-induced enzymatic activity inhibition in tyrosinase/ZnO NPs/SPCE biosensor for the detection of ppb levels of herbicide. *Sens. Actuators, B* **2015**, *219*, 171−178.
(58) Li, X.; Zhang, L.; Wei, X. A sensitive and renewable chlortoluron molecularly imprinted polymer sensor based on the gate-controlled catalytic electrooxidation of H_2O_2 on magnetic nano-NiO. *Electroanalysis* **2013**, *25* (5), 1286−1293, DOI: 10.1002/elan.201200428.
(59) Surribas, A.; Barthelmebs, L.; Noguer, T. Monoclonal Antibody-Based Immunosensor for the Electrochemical Detection of Chlortoluron Herbicide in Groundwaters. *Biosensors* **2021**, *11*, 513.
(60) Tsai, H.; Shaya, J.; Tesana, S.; Golovko, V. B.; Wang, S.; Liao, Y.; Lu, C.; Chen, C. Visible-Light Driven Photocatalytic Degradation of Pirimicarb by Pt-Doped AgInS2 Nanoparticle. *Catalysts* **2020**, *10* (8), No. 857, DOI: 10.3390/catal10080857.
(61) Babazadeh, S.; Moghaddam, P.; Keshipour, S.; Mollazade, K. Colorimetric sensing of imidacloprid in cucumber fruits using a graphene quantum dot/Au (III), chemosensor. *Sci. Rep.* **2020**, *10* (1), No. 14327.
(62) Dong, W.; Zhou, S.; Dong, Y.; Wang, J.; Gea, X.; Sui, L. The preparation of ethylenediamine-modified fluorescent carbon dots and their use in imaging of cells. *Luminescence* **2015**, *30*, 867−871.
(63) Chahal, S.; Macairan, J.; Yousefi, N.; Tufenkji, N.; Naccache, R. Green synthesis of carbon dots and their applications. *RSC Adv.* **2021**, *11*, 25354−25363.
(64) Yusuf, V. F.; Atulbhai, S. V.; Swapna, B.; Malek, N. I.; Kailasa, S. K. Recent developments in carbon dot-based green analytical methods: new opportunities in fluorescence assays of pesticides, drugs and biomolecules. *New J. Chem.* **2022**, *46*, 14287−14308.
(65) Wang, M.; Wan, Y.; Zhang, K.; Fu, Q.; Wang, L.; Zeng, J.; Xia, Z.; Gao, D. Green synthesis of carbon dots using the flowers of Osmanthus fragrans (Thunb.) Lour. as precursors: application in Fe^{3+} and ascorbic acid determination and cell imaging. *Anal. Bioanal. Chem.* **2019**, *411*, 2715−2727.
(66) Barchanska, H.; Kluza, A.; Krajczewska, K.; Maj, J. Degradation study of mesotrione and other triketone herbicides on soils and sediments. *J. Soils Sediments* **2016**, *16*, 125−133.
(67) Yin, P.; Zou, T.; Yao, G.; Li, S.; He, Y.; Li, G.; Li, D.; Tan, W.; Yang, M. In situ microwave-assisted preparation of NS-codoped carbon dots stabilized silver nanoparticles as an off-on fluorescent probe for trace Hg^{2+} detection. *Chemosphere* **2023**, *338*, No. 139451.
(68) Vadia, F. Y.; Ghosh, S.; Mehta, V. N.; Jha, S.; Malek, N. I.; Park, T. J.; Kailasa, S. K. Fluorescence "Turn OFF-ON" detection of Fe^{3+} and propiconazole pesticide using blue emissive carbon dots from lemon peel. *Food Chem.* **2023**, *428*, No. 136796.
(69) Yue, X.; Zhou, Z.; Wu, Y.; Jie, M.; Li, Yan.; Guo, H.; Bai, Y. Green carbon dotsbased fluorescent sensor for selective and visual detection of nitrite triggered by the nitrite-thiol reaction. *New J. Chem.* **2020**, *44*, 8503−8511.
(70) Praneerad, J.; Thongsai, N.; Supchocksoonthorn, P.; Kladsomboo, S.; Paoprasert, P. Multipurpose sensing applications of biocompatible radish-derived carbon dots as Cu^{2+} and acetic acid vapor sensors. *Spectrochim. Acta, Part A* **2019**, *211*, 59−70.
(71) Ding, H.; Yu, S.; Wei, J.; Xiong, H. Full-Color Light-Emitting Carbon Dots with a Surface-State-Controlled Luminescence Mechanism. *ACS Nano* **2016**, *10*, 484−491.
(72) Xu, H.; Yang, X.; Li, G.; Zhao, C.; Liao, X. Green Synthesis of Fluorescent Carbon Dots for Selective Detection of Tartrazine in Food Samples. *J. Agric. Food Chem.* **2015**, *63* (30), 6707−6714.

https://doi.org/10.1021/acsomega.3c07171
ACS Omega 2023, 8, 49115−49128